

Do image and video quality metrics model low-level human vision?

Dounia Hammou¹ Yancheng Cai¹ Pavan Madhusudanarao² Christos G. Bampis²

Rafał K. Mantiuk¹

¹University of Cambridge ²Netflix, Inc.

¹{dh706, yc613, rafal.mantiuk}@cl.cam.ac.uk ²{pmadhusudanarao, christosb}@netflix.com

Abstract

Image and video quality metrics, such as SSIM, LPIPS, and VMAF, are aimed to predict the perceived quality of the evaluated content and are often claimed to be “perceptual”. Yet, few metrics directly model human visual perception, and most rely on hand-crafted formulas or training datasets to achieve alignment with perceptual data. In this paper, we propose a set of tests for full-reference quality metrics that examine their ability to model several aspects of low-level human vision: contrast sensitivity, contrast masking, and contrast matching. The tests are meant to provide additional scrutiny for newly proposed metrics. We use our tests to analyze 33 existing image and video quality metrics and find their strengths and weaknesses, such as the ability of LPIPS and MS-SSIM to predict contrast masking and poor performance of VMAF in this task. We further find that the popular SSIM metric overemphasizes differences in high spatial frequencies, but its multi-scale counterpart, MS-SSIM, addresses this shortcoming. Such findings cannot be easily made using existing evaluation protocols.

1. Introduction

Image and video quality metrics, such as PSNR, SSIM [57], LPIPS [65], or VMAF [35], are widely used to validate the results of image reconstruction methods [22, 58], test and optimize image/video compression [67], and for a wide range of other applications. The development of quality metrics has been a long-term quest to make the metrics more “perceptual” and better aligned with human opinion scores, such as MOS [26], JND or JOD [42] values measured in quality assessment experiments. Here, we argue that a fully perceptual metric should also mimic human responses from psychophysical experiments that characterize human low-level vision, such as contrast detection, contrast discrimination, and contrast matching.

The gold standard for measuring metric performance has been to report a correlation between metric predictions and

human quality scores. The problem is that subjective quality scores are noisy [30, 44], differ between datasets [43], and are specific for the type of distortions found in a given dataset. For that reason, a metric that performs the best for one dataset can often show mediocre performance for another dataset. Furthermore, a single correlation value does not explain why a metric performs well or poorly.

In this paper, we introduce an alternative approach that lets us investigate the performance of quality metrics. We design tests that examine whether a metric models well-established characteristics of low-level human vision, such as detection of patterns of different frequency, luminance, and area (contrast sensitivity) [5, 8, 27, 46], discrimination of patterns mixed with background patterns (contrast masking) [18, 19, 60], detecting flicker (temporal contrast sensitivity) [10, 49], and estimating the magnitude of supra-threshold contrast [20, 53]. In our approach, we supply a quality metric with patterns that are often used in vision science to measure the performance of the visual system, such as Gabor patches or band-limited noise. We collect metric responses for a range of pattern parameters, such as a range of spatial frequencies and contrast magnitudes. The collected metric responses are then compared with psychophysical data or models that capture human vision characteristics. The outcome is a contour plot visualization that lets us understand the performance of a given metric, and also an aggregate alignment score that lets us measure how close the metric prediction is to the human data. Such an approach reveals an aspect of the quality metric performance that has been overlooked — whether the metrics that are claimed to be perceptual actually model low-level perception. Our analysis is meant to complement metric testing on subjective datasets, providing more insights into the strengths and weaknesses of a given quality metric.

The main contributions of this work are:

- A set of 11 tests that are used to analyze how well a quality metric can predict the characteristic of low-level vision.
- Analysis of 33 image and video quality metrics, showing how well each quality metric models low-level human vi-

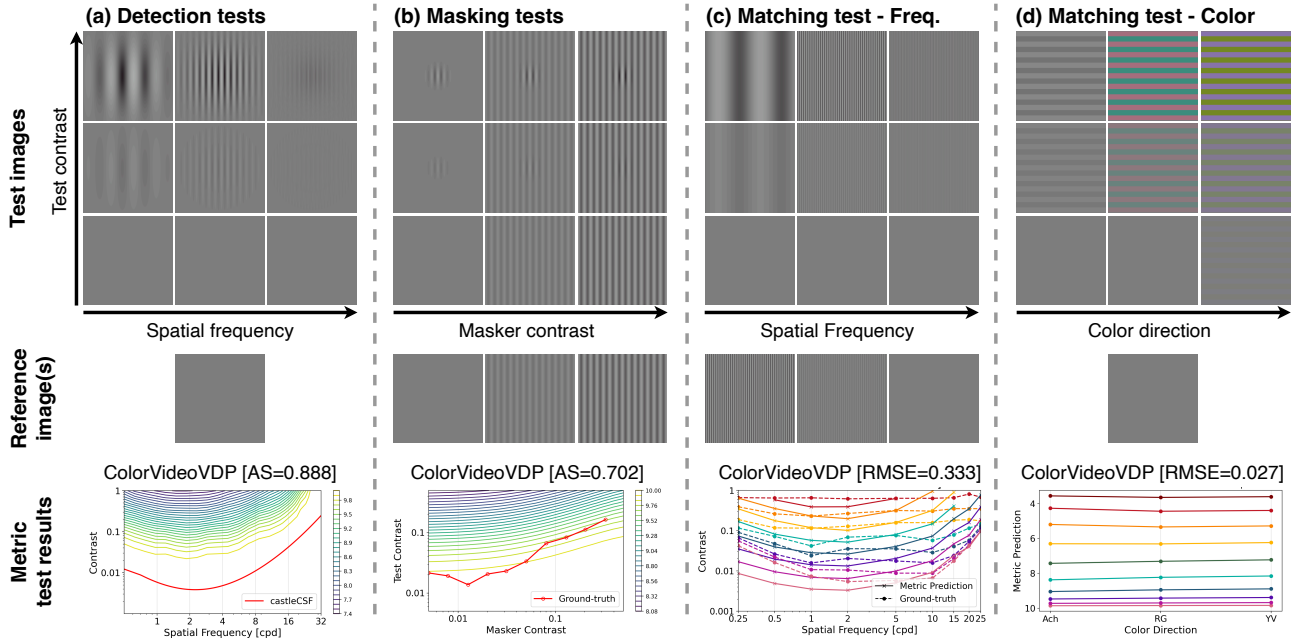


Figure 1. A representation of the methodologies employed to evaluate the metrics on the various tests (each in a column). The first row represents a grid of the test images. The second row represents the reference image(s) for each test. For tests where the reference image was a uniform field, we showcase only one image. The third row showcases the metric results on the specific test, for example, a contour plot for the detection test, as well as the performance score (an alignment score (AS) or RMSE).

sion.

2. Related work

The dominant methodology for testing image and video quality metrics is to compare the predictions with subjective data in terms of correlation coefficients (Pearson’s, Spearman’s, or Kendall’s coefficients) or root-mean-square-error (RMSE). The main weakness of such an approach is that it does not account for the measurement error associated with the subjective data (MOS, DMOS, JODs). Krasula et al. [30] addressed this shortcoming by posing the metrics’ task as a classification problem. Their method tests whether a metric can classify condition pairs into those that are of similar and different quality and then, for those that are of different quality, whether it can predict which one has a higher quality. More recently, Ragano et al. [44] proposed the Constrained Concordance Index (CCI), which measures the metric’s capability to accurately rank pairs where MOS has high precision and ignores the ones with uncertain MOS. All these measures help to better discriminate between metrics performance on a given dataset, but they provide little insight into why metrics perform poorly or well. Our tests are not meant to replace metric performance measures but to complement them by illustrating the strengths and weaknesses of the metrics.

Psychophysical stimuli were used before to calibrate

and test visual difference predictors: HDR-VDP-2 [36], FovVideoVDP [37], and ColorVideoVDP [39]. However, those works involved a limited range of such stimuli and lacked a comprehensive comparison with other quality metrics. ModelFest dataset [59] offers a set of 43 contrast discrimination stimuli for testing visual models. Alam et al. [3] created a dataset for local masking in natural images for testing contrast masking models. We do not use either of these datasets as they provide less structured data that is more difficult to visualize and interpret. Several studies investigated the presence of contrast sensitivity function (CSF) in neural networks [2, 34, 54]. Here, we argue that contrast sensitivity, while important, explains only human performance for very small contrast shown on uniform backgrounds. Therefore, in this work, we investigate both near-threshold and supra-threshold human vision characteristics (i.e., contrast masking and contrast matching). More recently, Cai et al. [11] used similar methods to ours to investigate whether computer vision foundation models learned low-level human vision features. Here, we focus on image and video quality metrics and customize our tests for such. For example, we include temporal (flicker) and color matching tests that are relevant for video and color metrics.

3. Proposed evaluation framework

Our testing methodology mimics psychophysical experiments used to collect low-level human vision data. For example, in a contrast detection psychophysical experiment, a participant is shown two intervals — one with a detection pattern at a given contrast and one without it — and then asked to determine in which interval the pattern was present. The outcome of such a measurement is a psychometric function describing the probability of detection as the function of contrast. Similarly, we test a quality metric by passing patterns of varying contrast as a test image (with stimulus), and a uniform field as a reference image (no stimulus, see (a) in Fig. 1). The metric predictions for patterns of different contrast and frequency form a 2D surface, which we can illustrate as a contour plot, as shown at the bottom of Fig. 1-(a). We can then compare the metrics’ responses with psychophysical data or models, such as a contrast sensitivity function (castleCSF) shown as a red solid line in Fig. 1-(a). A metric that correctly models contrast detection should have its contour lines aligned with the red line of the CSF.

Psychophysical experiments require stimuli calibrated in physical units — pixel values as luminance (cd/m^2) or CIE LMS cone responses, and image size in visual degrees. Some metrics (ColorVideoVDP, HDR-VDP, FLIP) let us pass the stimuli in physical units. However, most of the quality metrics ignore the physical image resolution and expect display-encoded images in sRGB color space as input. For that reason, we had to make a few assumptions and restrict the range of physical parameters. The physical resolution was assumed to be near 60 pixels per degree (ppd), which corresponds to the ITU-T BT.2100 recommendation for the FullHD television (3.2 display heights). This also corresponds to a 10” 1080p tablet seen from 40 cm. We varied this resolution in some tests to better reproduce high-frequency patterns. The display peak luminance was assumed to be $100 \text{ cd}/\text{m}^2$ (typical for desktop displays), and the mean luminance for most patterns was $21.4 \text{ cd}/\text{m}^2$. The patterns were generated in a linear color space (luminance or CIE 2006 LMS cone responses [15]) and then converted into the sRGB color space. Furthermore, we ensured that all images were passed to the metric either as floating point numbers or integers quantized to 16 bits to ensure minimal loss of information.

Our 11 tests can be grouped into three types, which we discuss next.

3.1. Detection tests

For the detection tests, the reference image was a uniform field, and the test image contained either a Gabor patch (contrast detection, see Fig. 1 column (a)) or a flickering disk (flicker detection). The equations for the different patterns and their parameters can be found in Sec. S1 of the

supplementary document. The resolution of the stimuli was 1920×1080 for the contrast detection and 256×256 for the flicker tests (for computational reasons). We used a recent contrast sensitivity model, castleCSF [5], to predict the detection threshold of the human observer. For the flicker test, we used elaTCSF [10]. Both models were shown to predict multiple psychophysical datasets and provide predictions for an average observer.

3.2. Contrast masking tests

For the masking tests, the reference image contained a masker, such as a sinusoidal grating (phase coherent masking) or a broadband noise (phase incoherent masking). The test images contained the same mask plus a Gabor patch of varying contrast — see column (b) in Fig. 1. The red lines represent user data collected in [18] for sinusoidal maskers, and in [19] for broadband noise. Similarly as for detection, we used contour plots to visualize metric responses.

3.3. Contrast matching tests

In the contrast matching experiment, an observer is asked to adjust the contrast of a test stimulus to match the perceived magnitude of contrast in a reference stimulus. The test and reference in our tests differ in spatial frequency (see column (c) in Fig. 1) or the modulation direction in a color space (e.g., the achromatic pattern is matched to the red-green pattern).

To mimic such a task with a quality metric, we want a metric prediction between a uniform field U and a sinusoidal test grating $S(\rho_t, c_t)$ of frequency ρ_t and contrast c_t to be the same as the metric prediction for the uniform field and a reference sinusoidal grating, $S(\rho_r, c_r)$:

$$Q(S(\rho_t, c_t), U) = Q(S(\rho_r, c_r), U) \quad (1)$$

where $Q(\cdot)$ is the metric prediction. The human data we use for comparison comes from the study of Georgeson and Sullivan [20], in which the reference was at $\rho_r = 5 \text{ cpd}$ (cycles per degree), and test frequencies varied between 0.25 and 25 cpd. Contrast matching data is visualized as lines of matching contrast, i.e., the lines that indicate contrast that appears the same across frequencies, as shown in the bottom of column (c) of Fig. 1.

For matching contrast across color directions, we used a square wave pattern and the matching data of Switkes et al. [53] — see column (d) in Fig. 1. Similarly to the previous test, we want the metric prediction for one color direction (e.g., red-green) to match the prediction for another direction (e.g., achromatic). The metrics results are visualized as a line connecting the metrics responses across the color directions, as shown in the bottom of column (d) of Fig. 1 (the line should be horizontal across color directions).

4. Experimental results and analysis

We evaluated 33 full-reference image and video quality metrics in 11 tests. Only full-reference metrics were included, as the tests require a comparison to a reference. The metrics were selected to represent different approaches to quality assessment: metrics based on traditional features, deep-learning, or psychophysical models; image and video metrics; luminance and color metrics. The tested metrics are listed in Tab. 1 and more details can be found in Sec. S3 of the supplementary document. For fairness, the detection of color patterns is evaluated only on color metrics and flicker only on video metrics.

Due to the large number of tests and metrics, we can include only the plots for the five most representative metrics in Fig. 2, however, our analysis considers all 33 tested metrics. We encourage the reader to refer to the supplementary HTML report for the detailed results of all metrics.

4.1. Contrast detection

One of the fundamental and well-studied visual characteristics is the eye’s ability to detect near-threshold contrast, known as contrast detection, and modeled by the contrast sensitivity function (CSF) [8, 27, 46]. The CSF explains the smallest contrast that an average observer’s eye can detect on a uniform background across spatial and temporal frequencies, color, luminance, and stimulus area [5].

Spatial frequency The contrast detection threshold for *achromatic* (grayscale) patterns is often measured across variations in spatial frequency. It follows a band-pass function, shown as a red line in Fig. 2-(a). The visual system exhibits the highest sensitivity (smallest contrast threshold) at intermediate frequencies between 2 and 4 cycles per visual degree (cpd) and a decrease in sensitivity at low and high frequencies. The drop in sensitivity at low spatial frequencies is attributed to the lateral inhibition mechanism [8] and to the optical limitations of the human eye [12] at high frequencies. When a pattern is modulated also in the temporal domain (flickers over time), the attenuation at low frequencies is reduced, and the sensitivity curve shows a low-pass characteristic across spatial frequencies [29].

The contour plots in row (a) of Fig. 2 and the supplementary HTML report show that very few metrics can well predict contrast sensitivity. Some metrics, such as sCIELab and FLIP, employ a simplified low-pass variant of the CSF, meaning that they are too sensitive to low-frequency distortions. SSIM is the most sensitive at the highest frequencies, contrary to the CSF. This problem seems to be resolved in MS-SSIM, which has a band-pass response. Deep learning metrics, such as DISTS, WaDIQaM, AHIQ, TOPIQ, DeepDC, or LPIPS variants, show erratic responses that do not align well with the CSF (red line). The best align-

ment can be observed for ColorVideoVDP and HDR-VDP-3, though this is unsurprising for the former as it is based on castleCSF, which we use as reference human data. Note that for most metrics, there is a gap between the lowest contour line and the red line of the CSF. This is because CSF provides a very low threshold that can be achieved only in ideal conditions (full adaptation, a pattern on a uniform field), while metrics are calibrated to predict clearly visible distortions, which tend to have higher contrast.

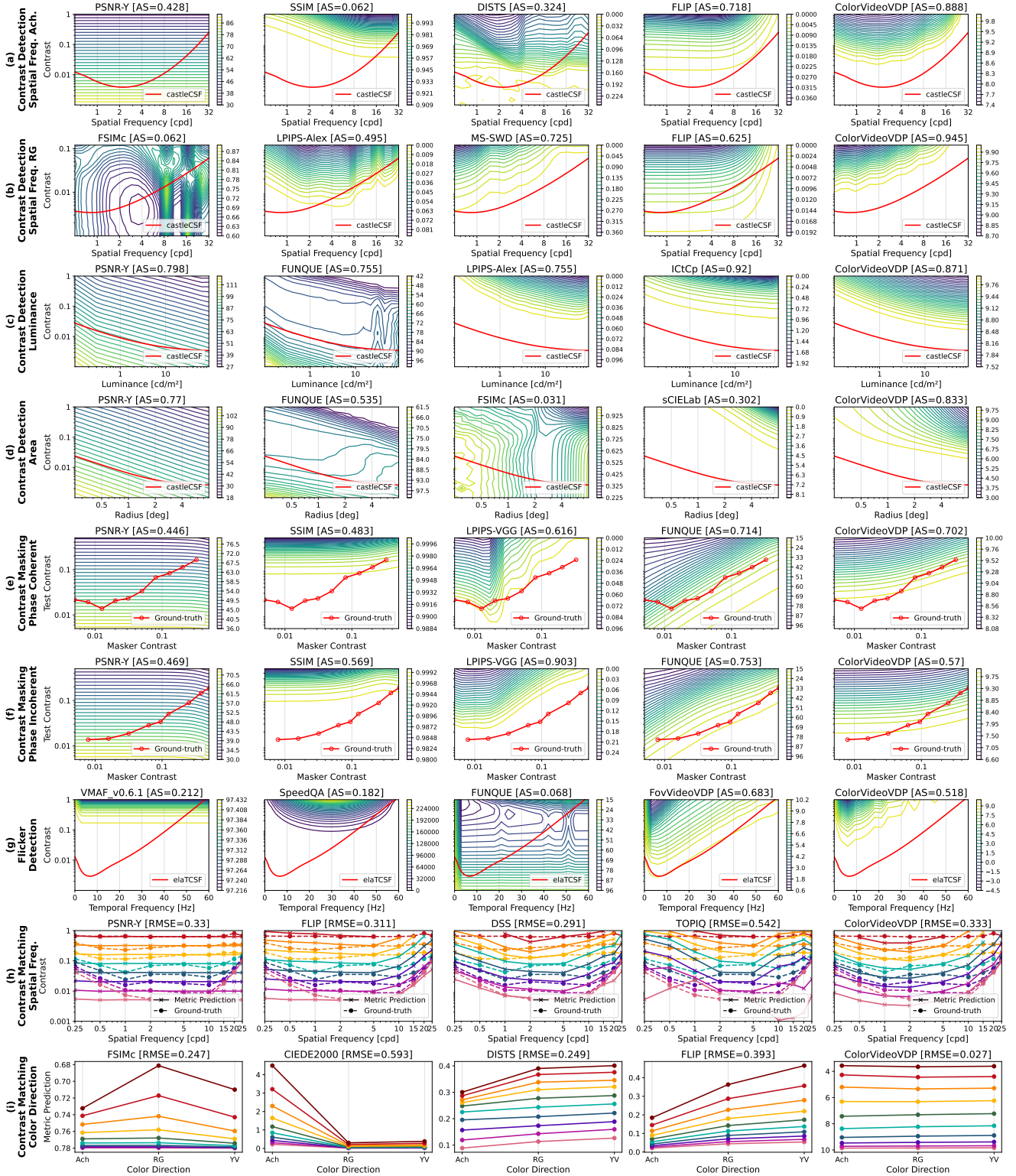
We also test video metric responses for spatio-temporal patterns, though those are shown only in the supplementary HTML report. This is tested for the temporal frequency of 8 Hz, which corresponds to the peak sensitivity of the visual system. The contour plots show that only ColorVideoVDP and FovVideoVDP model the expected low-pass characteristic, though FovVideoVDP shows a rather erratic response. VMAF cannot differentiate between temporal frequencies and gives the same response as for a static pattern. Other video metrics fail to predict spatio-temporal contrast sensitivity.

Contrast sensitivity for *chromatic* patterns, red-green (RG) and yellow-violet (YV) [51], follows approximately a low-pass shape, as the inhibition at low spatial frequencies is weaker in chromatic pathways [28]. We analyze only the RG color direction as YV shows similar trends.

Row (b) in Fig. 2 shows that FSIMc fails to account for the CSF, which is partially due to the subsampling used in this metric. Some deep learning metrics, such as LPIPS-Alex, result in a band-pass characteristic, which is inconsistent with the chromatic CSF. However, MS-SWD (deep-learning-based color measure) shows an expected low-pass response. FLIP shows the expected low-pass response but is too sensitive between 2 and 16 cpd. ColorVideoVDP follows the chromatic CSF but with lower sensitivity and small variation across the spatial frequencies (most likely caused by operating on a fixed number of Laplacian pyramid levels).

Luminance The human visual system’s sensitivity to contrast is dependent on the luminance of the stimuli. At dim luminance levels (up to around 10 cd/m^2), the sensitivity follows the Devries-Rose law, where the sensitivity proportionally increases with the square root of retinal illuminance. At brighter luminance levels, the sensitivity follows Weber’s law, becoming independent of the luminance [48].

The majority of metrics expect input images to be provided in the sRGB space (rec.709 color primaries, approx. gamma of 2.2). As seen in the example of PSNR-Y response in row (c) of Fig. 2, this color space provides encoding that is mostly well-aligned with the human contrast sensitivity, with the exception of higher luminance levels, for which the sensitivity is higher than expected. Nev-



ertheless, some metrics’ features, such as those used in FUNQUE, may disturb the approximate perceptual linearity of the sRGB space, resulting in predictions that are less aligned with the CSF. Most deep-learning-based metrics (such as LPIPS-Alex) show good alignment with the CSF; however, similarly to previous tests, they are less sensitive to near-threshold contrast, as such contrast is less likely to be learned when not present in the training dataset. The metrics that operate on physical or colorimetric pixel values, such as HDR-VDP-3, CIEDE2000, or ICtCp, perform the best at modeling the luminance sensitivity, as they operate in perceptually uniform spaces.

Area Contrast is more detectable when it occupies a larger area, and such an increase can be observed up to a saturation point known as the critical area [47]. Metrics also pool the contribution of the distortions over the image, but such a pooling mechanism differs between the metrics.

Row (d) in Fig. 2 and the contour plots in the supplementary HTML report show the increased response of most metrics with the size of the stimulus, but for some metrics this response is unstable at low contrast (VIFp, SpeedQA, FUNQUE) or even non-monotonic (FSIMc, VSI). The main difference between the metrics is in the slope of the response. For example, PSNR-Y has an identical pooling mechanism slope as CSF for small sizes, but it does not model saturation at the critical area. FLIP and sCIELab have stronger (steeper) integration than the CSF. ColorVideoVDP, HaarPSI, and FovVideoVDP have the slope matching that of the CSF, though they are less sensitive at low contrast.

4.2. Contrast masking

Contrast detection, discussed in the previous section, applies to the case when a detected pattern (e.g., distortion) is shown on a uniform background. Such a case, however, is rare in natural images, as most distortions are mixed with image content, and the visibility of a distortion is masked by textures and patterns present in the image. This phenomenon is known as contrast masking in the human vision literature [60] and was found to be the strongest when the masking pattern has a similar spatial frequency and orientation as the detected pattern [18, 52]. Contrast masking explains how large the contrast of a pattern must be to be detected in the presence of a masker of a given contrast. The two examples of such masking characteristics are shown as red lines in rows (e) (data from [18]) and (f) (data from [19]) of Fig. 2. The test contrast required for detection increases once the masker’s contrast is above the detection threshold [16]. The difference between rows (e) and (f) is that in row (e) we use a sinusoidal masker (phase coherent with the detected Gabor patch, see Fig. 1 column (c)) that is causing a facilitation (a “dipper” effect) of detection near the de-

tection threshold, while in (f) the masker is a broadband noise (phase incoherent with the detected Gabor patch) that causes the facilitation to disappear.

The results for the contrast masking test can be found in rows (e) and (f) of Fig. 2 and in the supplementary HTML report. Based on those, we can divide the metrics into those that do not model masking at all (PSNR-Y, SpeedQA, FLIP, VMAF, AHIQ, TOPIQ, ST-LPIPS-Alex), those that model the masking for higher supra-threshold contrast as a straight increase of the discrimination threshold (FUNQUE, HDR-VDP-3, VSI), and those that also model reduced masking at low contrast (ColorVideoVDP, MS-SSIM, LPIPS, DISTs). The metrics based on the VGG (LPIPS-VGG and DISTs) and AlexNet (DeepDC) architectures also show a dip in the contours, similar to the facilitation effect, but it appears at a higher-than-expected contrast. It is interesting to notice VMAF and ST-LPIPS, which perform well on certain image quality dataset, do not learn contrast masking, which could indicate overfitting on those datasets. In contrast, metrics based on deep features (LPIPS and DISTs) show remarkably good performance. Similar performance, however, can be also achieved with relatively simple formulas found in SSIM and MS-SSIM metrics.

4.3. Flicker detection

A flicker (rapid change of contrast/luminance over time) is a salient artifact that a video quality metric should be able to detect. Flicker detection in human vision depends on temporal frequency, luminance, size of a flickering pattern, and the position in the visual field (eccentricity) [40], but here we focus only on the temporal frequency. The human sensitivity to flicker has a band-pass characteristic with a peak at 8 Hz (see the red line in row (g) in Fig. 2). When the critical flicker fusion frequency (CFF) is reached, the flicker is no longer perceived (is fused into a steady field due to the persistence of vision) [23].

We test how well metrics can predict the sensitivity to flicker, including flicker fusion. Our test video contains a disk modulated over time at varying frequencies (sinusoidal modulation) and the reference video is a uniform field. *elaTCSF* model [10] provides human sensitivity data for such a flickering disk (red line in row (g) of Fig. 2). Although multiple video quality metrics claim to model temporal distortions, only FovVideoVDP and ColorVideoVDP were able to predict the sensitivity to flicker. A part of the reason is that video quality metrics rarely consider more than a couple of frames when evaluating temporal distortions. Such a small filter is unable to differentiate between different temporal frequencies.

4.4. Supra-threshold contrast matching

Matching across spatial frequencies Many quality metrics incorporate the models of contrast sensitivity (CSF) and

ensure band-pass (or low-pass) response across the spatial frequencies. However, the CSF predicts the visibility of only a small contrast that is close to the detection threshold. Georgeson and Sullivan [20] showed that for large contrast that is much above the detection threshold, there is much less variation in the magnitude of perceived contrast across the spatial frequencies. Their contrast-matching data is shown as dashed lines in row (h) of Fig. 2. The lines have a U-shape for small contrast, suggesting that both low and high frequencies need a higher contrast to match the perceived magnitude of medium frequencies. However, the dashed lines are almost flat at high contrast, indicating no difference in contrast perception across spatial frequencies. This phenomenon is known as *contrast constancy*.

The results of contrast matching for each metric are shown in row (h) Fig. 2 and supplementary HTML report as continuous lines, with different colors assigned to different contrast magnitudes. Note the missing segments of the line mean that contrast could not be matched to the reference.

None of the quality metrics we tested could predict contrast constancy — the “flattening” of the perceived contrast at large contrast values. In terms of contrast matching results, the quality metrics can be split into three groups. The first group is the metrics that do not contain any spatial processing, such as PSNR-Y or CIEDE2000. Those metrics maintain contrast constancy at large contrast but obviously cannot model the reduced perceived magnitude of small and medium contrast (their lack the U-shape in row (h) of Fig. 2). The second group is the metrics that explicitly employ a contrast sensitivity function as a low-pass filter (sCIELab or FLIP) or a band-pass filter (ColorVideoVDP, HDR-VDP-3), or employ a frequency decomposition that modulates sensitivity with frequencies (MS-SSIM, DSS, HaarPSI, NLPD). For all metrics in this group, the lines of matching contrast are parallel to each other and show little flattening for high contrast. ColorVideoVDP and HDR-VDP-3 predict the CSF peak at lower frequencies and, therefore, show higher misalignment with the data of Georgeson and Sullivan. The final group is the metrics that fail to maintain contrast response across frequencies and show very erratic behavior (VIFp, FSIMc, VSI, TOPIQ, LPIPS-VGG).

Matching across color directions We want metrics to correctly estimate the magnitude of perceived contrast not only across spatial frequencies but also across different color directions. To test for that, we rely on the data of Switkes and Crognale [53], who matched contrast along different contrast modulation directions in a color space, as shown in column (d) of Fig. 1. The data allowed us to generate square-wave gratings in the achromatic (grayscale), red-green, and yellow-violet color directions so that the perceived magnitude of contrast for each is matched. In row (i)

of Fig. 2, we plot the metrics’ response of each such triplet, connected by a line. If a metric correctly matches contrast across color directions, the response of the metric should be the same, and the lines should be horizontal.

The plots in row (i) of Fig. 2 and in the supplementary HTML report show that some metrics do not balance the perceived contrast magnitudes well. For example, CIEDE2000 and HyAB are much more sensitive to achromatic than to chromatic contrast. The opposite can be observed for sCIELab, FLIP, and ICtCp metrics. It must be noted that metrics based on color difference formulas (e.g., CIEDE2000) were calibrated and intended for only small, near-threshold color differences, while our test contains large supra-threshold differences. All deep learning-based metrics tend to overemphasize chromatic differences (MS-SWD, DeepDC, LPIPS both variants). ColorVideoVDP achieved the best match in this test, followed by FSIMc (good match at low contrast) and DISTs (overemphasized chromatic differences).

5. Aggregate performance measures

In addition to contour plots, we also calculate summative performance measures of alignment score and RMSE. Those are identical as in [10] and also explained in Sec. S2 of the supplementary document. Such measures lack the interpretation and detail provided by the contour plots but give a high level overview and facilitate comparison across multiple metrics.

Tab. 1 shows the alignment scores (the higher, the better) for contrast detection and masking and RMSE (the lower, the better) for contrast matching. As expected, the visual difference predictors that explicitly model low-level vision show the best alignment with the human data. LPIPS variants and DISTs stand out as those that model contrast masking well. MS-SWD models the detection of both chromatic and achromatic patterns well. Only FovVideoVDP and ColorVideoVDP model flicker. The RMSE values for contrast matching do not explain the performance well as they indicate that the metrics without spatial processing (e.g., PSNR-Y, CIEDE2000) perform the best. This is because those metrics have flat contrast response across all frequencies, which happen to capture contrast constancy at high contrast values — see row (h) of Fig. 2.

6. Discussion and conclusions

The methodology proposed in this paper let us test whether quality metrics model the low-level characteristics of the visual system. This led us to multiple interesting and new observations about the performance of widely used quality metrics. For example, we found that many deep learning metrics excel in modeling contrast masking (e.g., LPIPS, DISTs) even though they have never been trained on such

Table 1. Alignment scores \uparrow (contrast detection, masking and flicker) and RMSE \downarrow (contrast matching) for all tested metrics. The colored background denotes the quantile across all the tested metrics: green — top 25%, yellow — 25-50%, orange 50-75%, red — bottom 25%. An empty cell indicates that the metric does not offer color or temporal processing or the score could not be computed. (*) The metric returned identical values, and correlation could not be computed.

Metric		Contrast Detection						Contrast Masking		Flicker Detection	Contrast Matching	
		Spatial Freq. Ach.	Spatial Freq. RG	Spatial Freq. YV	Spatial Freq. Transient	Luminance	Area	Phase Coherent	Phase Incoherent		Spatial Freq.	Color Direction
Traditional metrics	PSNR-Y	0.428	-	-	-	0.798	0.77	0.446	0.469	-	0.33	-
	SSIM [57]	0.062	-	-	-	0.299	0.134	0.483	0.569	-	0.507	-
	MS-SSIM [56]	0.682	-	-	-	0.23	0.091	0.559	0.535	-	0.23	-
	GMSD [61]	0.386	-	-	-	0.798	0.886	0.526	0.554	-	0.459	-
	MS-GMSD [62]	0.407	-	-	-	0.798	0.897	0.571	0.528	-	0.356	-
	VIFp [50]	0.019	-	-	-	0.087	0.054	0.297	0.38	-	0.586	-
	DSS [6]	0.489	-	-	-	0.653	0.954	0.746	0.614	-	0.291	-
	NLPD [32]	0.484	-	-	-	0.798	0.755	0.531	0.487	-	0.279	-
Traditional color metrics	FSIMc [63]	0.039	0.062	0.04	-	0.077	0.031	0.642	0.633	-	-	0.247
	VSI [64]	0.134	0.169	0.193	-	0.222	0.092	0.629	0.534	-	-	0.458
	MDSI [41]	0.538	0.643	0.621	-	0.798	0.847	0.484	0.53	-	0.602	0.337
	HaarPSI [45]	0.504	0.623	0.573	-	0.877	0.89	0.614	0.484	-	0.385	0.344
	sCIELab [66]	0.635	0.562	0.522	-	0.734	0.302	0.447	0.476	-	0.403	0.45
	FLIP [4]	0.718	0.625	0.695	-	0.696	0.201	0.449	0.477	-	0.311	0.393
Color difference measures	CIEDE2000 [14]	0.428	0.438	0.403	-	0.92	0.302	0.452	0.474	-	0.329	0.593
	HyAB [1]	0.428	0.438	0.403	-	0.733	0.302	0.447	0.472	-	0.329	0.593
	ICtP [25]	0.427	0.438	0.403	-	0.92	0.21	0.446	0.467	-	0.329	0.426
	MS-SWD [24]	0.654	0.725	0.831	-	0.736	0.334	0.44	0.689	-	0.401	0.685
	WaDIQaM [9]	0.16	0.199	0.15	-	0.05	0.125	0.159	0.037	-	-	0.393
Deep-learning based metrics	LPIPS-Alex [65]	0.393	0.495	0.45	-	0.755	0.793	0.879	0.839	-	0.408	0.457
	LPIPS-VGG [65]	0.291	0.371	0.33	-	0.867	0.831	0.616	0.903	-	0.562	0.512
	ST-LPIPS-Alex [21]	0.396	0.426	0.408	-	0.728	0.78	0.495	0.408	-	0.499	0.652
	DISTS [17]	0.324	0.454	0.389	-	0.187	0.447	0.561	0.798	-	0.454	0.249
	AHIQ [31]	0.358	0.219	0.297	-	0.015	0.646	0.399	0.552	-	-	0.508
	TOPIQ [13]	0.309	0.474	0.561	-	0.0	0.412	0.101	0.096	-	0.542	0.324
	DeepDC [68]	0.193	0.328	0.272	-	0.724	0.238	0.385	0.481	-	0.515	0.287
	Video metrics	VMAF v0.6.1 [35]	0.577	-	-	0.752	0.216	0.203	0.549	0.494	0.212	0.373
SpeedQA [7]		0.285	-	-	0.076	0.847	0.098	0.111	0.556	0.182	1.775	-
FUNQUE [55]		0.434	-	-	0.405	0.755	0.535	0.714	0.753	0.068	0.52	-
Visual difference predictors	MAD [33]	0.125	-	-	-	0.0 (*)	0.281	0.528	0.42	-	0.861	-
	HDR-VDP-3 [38]	0.695	-	-	-	0.977	0.825	0.861	0.897	-	0.372	-
	FovVideoVDP [37]	0.507	-	-	0.5	0.974	0.914	0.934	0.538	0.683	0.573	-
	ColorVideoVDP [39]	0.888	0.945	0.956	0.9	0.871	0.833	0.702	0.57	0.518	0.333	0.027

data. That popular SSIM overemphasized differences in higher frequencies, contrary to contrast detection and contrast matching psychophysical data. That VMAF, which is one of the most widely used video metrics, poorly models the effect of contrast masking. Or that color difference formulas (CIEDE2000, HyAB) underestimate color differences for large (supra-threshold) contrast levels. We hope that our methodology and software will help in scrutinizing the performance of existing and newly proposed metrics.

It is important to state that a good performance in our low-level human vision tests may not be a required or sufficient condition for a metric to perform well across the applications. For example, SSIM is arguably better at capturing perceived quality than PSNR, but Tab. 1 shows that for all tests except contrast masking, PSNR-Y is better aligned with the visual system. Instead, we put an argument that a metric that performs well in our low-level vision tests has a better chance to generalize to new and unseen types of distortions. Our method is also limited to full-reference metrics that quantify the fidelity to the reference. Our method cannot be used with no-reference metrics that assess other aspects of quality, such as aesthetics or how well the distri-

bution of results aligns with the distribution of natural images (e.g., FID metric).

References

- [1] Saeedeh Abasi, Mohammad Amani Tehran, and Mark D Fairchild. Distance metrics for very large color differences. *Color Research & Application*, 45(2):208–223, 2020. 8
- [2] Arash Akbarinia, Yaniv Morgenstern, and Karl R. Gegenfurtner. Contrast sensitivity function in deep networks. *Neural Networks*, 164:228–244, 2023. 2
- [3] M. M. Alam, K. P. Vilankar, David J Field, and Damon M Chandler. Local masking in natural images: A database and analysis. *Journal of Vision*, 14(8):22–22, 2014. Citation Key: Alam2014. 2
- [4] Pontus Andersson, Jim Nilsson, Tomas Akenine-Möller, Magnus Oskarsson, Kalle Åström, and Mark D Fairchild. FLIP: A difference evaluator for alternating images. *Proc. ACM Comput. Graph. Interact. Tech.*, 3(2):15–1, 2020. 8
- [5] Maliha Ashraf, Rafał K Mantiuk, Alexandre Chapiro, and Sophie Wuergler. castleCSF—A contrast sensitivity function of color, area, spatiotemporal frequency, luminance and eccentricity. *J. Vis.*, 24(4):5–5, 2024. 1, 3, 4
- [6] Amnon Balanov, Arik Schwartz, Yair Moshe, and Nimrod

- Peleg. Image quality assessment based on dct subband similarity. In *ICIP*, pages 2105–2109. IEEE, 2015. 8
- [7] Christos G Bampis, Praful Gupta, Rajiv Soundararajan, and Alan C Bovik. SpEED-QA: Spatial efficient entropic differencing for image and video quality. *IEEE signal processing letters*, 24(9):1333–1337, 2017. 8
- [8] Peter GJ Barten. *Contrast sensitivity of the human eye and its effects on image quality*. SPIE press, 1999. 1, 4
- [9] Sebastian Bosse, Dominique Maniry, Klaus-Robert Müller, Thomas Wiegand, and Wojciech Samek. Deep neural networks for no-reference and full-reference image quality assessment. *IEEE TIP*, 27(1):206–219, 2017. 8
- [10] Yancheng Cai, Ali Bozorgian, Maliha Ashraf, Robert Wanat, and K Rafał Mantiuk. elatCSF: A temporal contrast sensitivity function for flicker detection and modeling variable refresh rate flicker. In *SIGGRAPH Asia 2024 Conference Papers*, pages 1–11, 2024. 1, 3, 6, 7
- [11] Yancheng Cai, Fei Yin, Dounia Hammou, and Rafał Mantiuk. Do computer vision foundation models learn the low-level characteristics of the human visual system? (arXiv:2502.20256), 2025. arXiv:2502.20256 [cs]. 2
- [12] FW Campbell and DG Green. Optical and retinal factors affecting visual resolution. *The J. physiology*, 181(3):576, 1965. 4
- [13] Chaofeng Chen, Jiadi Mo, Jingwen Hou, Haoning Wu, Liang Liao, Wenxiu Sun, Qiong Yan, and Weisi Lin. TOPIQ: A top-down approach from semantics to distortions for image quality assessment. *IEEE TIP*, 2024. 8
- [14] CIE. CIE 015: 2018 Colorimetry, 2018. 8
- [15] CIE170-1:2006. *Fundamental chromacity diagram with psychological axes - part 1*. 2016. Citation Key: CIE170-1:20062016. 3
- [16] S.J. Daly. *Visible differences predictor: an algorithm for the assessment of image fidelity*, page 179–206. MIT Press, 1993. 6
- [17] Keyan Ding, Kede Ma, Shiqi Wang, and Eero P Simoncelli. Image quality assessment: Unifying structure and texture similarity. *IEEE TPAMI*, 44(5):2567–2581, 2020. 8
- [18] John M Foley. Human luminance pattern-vision mechanisms: masking experiments require a new model. *Journal of the Optical Society of America A*, 11(6):1710–1719, 1994. 1, 3, 6
- [19] Karl R Gegenfurtner and Daniel C Kiper. Contrast detection in luminance and chromatic noise. *Journal of the Optical Society of America A*, 9(11):1880–1888, 1992. 1, 3, 6
- [20] MA Georgeson and GD Sullivan. Contrast constancy: deblurring in human vision by spatial frequency channels. *The J. physiology*, 252(3):627–656, 1975. 1, 3, 7
- [21] Abhijay Ghildyal and Feng Liu. Shift-tolerant perceptual similarity metric. In *ECCV*, pages 91–107. Springer, 2022. 8
- [22] Param Hanji, Rafał Mantiuk, Gabriel Eilertsen, Saghi Hajisharif, and Jonas Unger. Comparison of single image HDR reconstruction methods—the caveats of quality assessment. In *ACM SIGGRAPH 2022 conference proceedings*, pages 1–8, 2022. 1
- [23] E Hartmann, B Lachenmayr, and H Brettel. The peripheral critical flicker frequency. *Vis. Res.*, 19(9):1019–1023, 1979. 6
- [24] Jiaqi He, Zhihua Wang, Leon Wang, Tsein-I Liu, Yuming Fang, Qilin Sun, and Kede Ma. Multiscale sliced Wasserstein distances as perceptual color difference measures. In *ECCV*, pages 1–18, 2024. 8
- [25] ITU-R. BT.2124-0: Objective metric for the assessment of the potential visibility of colour differences in television, 2019. 8
- [26] ITU-T. P.910: Subjective video quality assessment methods for multimedia applications, 2023. 1
- [27] DH Kelly. Motion and vision. I. Stabilized images of stationary gratings. *JOSA*, 69(9):1266–1274, 1979. 1, 4
- [28] DH Kelly. Spatiotemporal variation of chromatic and achromatic contrast thresholds. *JOSA*, 73(6):742–750, 1983. 4
- [29] D. H. Kelly. Motion and vision II Stabilized spatio-temporal threshold surface. *JOSA*, 69(10):1340, 1979. Citation Key: Kelly1979. 4
- [30] Lukas Krasula, Karel Fliegel, Patrick Le Callet, and Milos Klima. On the accuracy of objective image and video quality models: New methodology for performance evaluation. In *QoMEX*, page 1–6, Lisbon, Portugal, 2016. IEEE. 1, 2
- [31] Shanshan Lao, Yuan Gong, Shuwei Shi, Sidi Yang, Tianhe Wu, Jiahao Wang, Weihao Xia, and Yujiu Yang. Attention help CNNs see better: Attention-based hybrid image quality assessment network. In *CVPR*, pages 1140–1149, 2022. 8
- [32] Valero Laparra, Johannes Ballé, Alexander Berardino, and Eero P Simoncelli. Perceptual image quality assessment using a normalized laplacian pyramid. *Electronic Imaging*, 28: 1–6, 2016. 8
- [33] Eric C Larson and Damon M Chandler. Most apparent distortion: full-reference image quality assessment and the role of strategy. *Journal of electronic imaging*, 19(1):011006–011006, 2010. 8
- [34] Qiang Li, Alex Gomez-Villa, Marcelo Bertalmío, and Jesús Malo. Contrast sensitivity functions in autoencoders. *Journal of Vision*, 22(6):8, 2022. 2
- [35] Zhi Li, Christos Bampis, Julie Novak, Anne Aaron, Kyle Swanson, Anush Moorthy, and JD Cock. VMAF: The journey continues. *Netflix Technology Blog*, 25(1), 2018. 1, 8
- [36] Rafał Mantiuk, Kil Joong Kim, Allan G Rempel, and Wolfgang Heidrich. HDR-VDP-2: A calibrated visual metric for visibility and quality predictions in all luminance conditions. *ACM TOG*, 30(4):1–14, 2011. 2
- [37] Rafał K Mantiuk, Gyorgy Denes, Alexandre Chapiro, Anton Kaplanyan, Gizem Rufo, Romain Bachy, Trisha Lian, and Anjul Patney. FovVideoVDP: A visible difference predictor for wide field-of-view video. *ACM TOG*, 40(4):1–19, 2021. 2, 8
- [38] Rafał K Mantiuk, Dounia Hammou, and Param Hanji. HDR-VDP-3: A multi-metric for predicting image differences, quality and contrast distortions in high dynamic range and regular content. *arXiv preprint arXiv:2304.13625*, 2023. 8
- [39] Rafał K. Mantiuk, Param Hanji, Maliha Ashraf, Yuta Asano, and Alexandre Chapiro. ColorVideoVDP: A visual difference predictor for image, video and display distortions. *ACM TOG*, 43(4), 2024. 2, 8

- [40] Nj Miller, Fa Leon, J Tan, and L Irvin. Flicker: A review of temporal light modulation stimulus, responses, and measures. *Lighting Research & Technology*, 55(1):5–35, 2023. 6
- [41] Hossein Ziaei Nafchi, Atena Shahkolaei, Rachid Hedjam, and Mohamed Cheriet. Mean deviation similarity index: Efficient and reliable full-reference image quality evaluator. *IEEE Access*, 4:5579–5590, 2016. 8
- [42] Maria Perez-Ortiz and Rafal K. Mantiuk. A practical guide and software for analysing pairwise comparison experiments. (arXiv:1712.03686), 2017. arXiv:1712.03686 [cs, stat]. 1
- [43] Maria Perez-Ortiz, Aliaksei Mikhailiuk, Emin Zerman, Vedad Hulusic, Giuseppe Valenzise, and Rafal K. Mantiuk. From pairwise comparisons and rating to a unified quality scale. *IEEE Transactions on Image Processing*, 29:1139–1151, 2020. 1
- [44] Alessandro Ragano, Helard Becerra Martinez, and Andrew Hines. Beyond correlation: Evaluating multimedia quality models with the constrained concordance index. *IEEE Transactions on Multimedia*, page 1–13, 2025. 1, 2
- [45] Rafael Reisenhofer, Sebastian Bosse, Gitta Kutyniok, and Thomas Wiegand. A Haar wavelet-based perceptual similarity index for image quality assessment. *Signal Processing: Image Communication*, 61:33–43, 2018. 8
- [46] John G Robson. Spatial and temporal contrast-sensitivity functions of the visual system. *JOSA*, 56(8):1141–1142, 1966. 1, 4
- [47] Jyrki Rovamo, Olavi Luntinen, and Risto Näsänen. Modelling the dependence of contrast sensitivity on grating area and spatial frequency. *Vis. Res.*, 33(18):2773–2788, 1993. 6
- [48] Jyrki Rovamo, Juvi Mustonen, and Risto Näsänen. Neural modulation transfer function of the human visual system at various eccentricities. *Vis. Res.*, 35(6):767–774, 1995. 4
- [49] Michele Rucci, Ehud Ahissar, and David Burr. Temporal coding of visual space. *Trends in cognitive sciences*, 22(10):883–895, 2018. 1
- [50] Hamid R Sheikh and Alan C Bovik. Image information and visual quality. *IEEE TIP*, 15(2):430–444, 2006. 8
- [51] Andrew Stockman, David H Brainard, et al. Color vision mechanisms. *The Optical Society of America handbook of optics*, 3:11–1, 2010. 4
- [52] C. F. Stromeyer and B. Julesz. Spatial-frequency masking in vision: Critical bands and spread of masking. *Journal of the Optical Society of America*, 62(10):1221, 1972. Citation Key: stromeyer1972spatial. 6
- [53] Eugene Switkes and Michael A Crognale. Comparison of color and luminance contrast: apples versus oranges? *Vis. Res.*, 39(10):1823–1831, 1999. 1, 3, 7
- [54] Taimoor Tariq, Okan Tarhan Tursun, Munchurl Kim, and Piotr Didyk. Why are deep representations good perceptual quality features? In *ECCV*, pages 445–461. Springer, 2020. 2
- [55] Abhinav K Venkataramanan, Cosmin Stejerean, and Alan C Bovik. FUNQUE: Fusion of unified quality evaluators. In *ICIP*, pages 2147–2151. IEEE, 2022. 8
- [56] Zhou Wang, Eero P Simoncelli, and Alan C Bovik. Multiscale structural similarity for image quality assessment. In *Asilomar Conference on Signals, Systems & Computers*, pages 1398–1402. IEEE, 2003. 8
- [57] Zhou Wang, Alan C Bovik, Hamid R Sheikh, and Eero P Simoncelli. Image quality assessment: from error visibility to structural similarity. *IEEE TIP*, 13(4):600–612, 2004. 1, 8
- [58] Zhihao Wang, Jian Chen, and Steven CH Hoi. Deep learning for image super-resolution: A survey. *IEEE TPAMI*, 43(10):3365–3387, 2020. 1
- [59] A.B. Watson and A.J. Ahumada Jr. A standard model for foveal detection of spatial contrast. *Journal of Vision*, 5(9):717–740, 2005. Citation Key: Watson2005. 2
- [60] Andrew B Watson and Joshua A Solomon. Model of visual contrast gain control and pattern masking. *Journal of the optical society of America A*, 14(9):2379–2391, 1997. 1, 6
- [61] Wufeng Xue, Lei Zhang, Xuanqin Mou, and Alan C Bovik. Gradient magnitude similarity deviation: A highly efficient perceptual image quality index. *IEEE TIP*, 23(2):684–695, 2013. 8
- [62] Bo Zhang, Pedro V Sander, and Amine Bermak. Gradient magnitude similarity deviation on multiple scales for color image quality assessment. In *ICASSP*, pages 1253–1257. IEEE, 2017. 8
- [63] Lin Zhang, Lei Zhang, Xuanqin Mou, and David Zhang. FSIM: A feature similarity index for image quality assessment. *IEEE TIP*, 20(8):2378–2386, 2011. 8
- [64] Lin Zhang, Ying Shen, and Hongyu Li. VSI: A visual saliency-induced index for perceptual image quality assessment. *IEEE TIP*, 23(10):4270–4281, 2014. 8
- [65] Richard Zhang, Phillip Isola, Alexei A Efros, Eli Shechtman, and Oliver Wang. The unreasonable effectiveness of deep features as a perceptual metric. In *CVPR*, 2018. 1, 8
- [66] Xuemei Zhang, Brian A Wandell, et al. A spatial extension of CIELAB for digital color image reproduction. In *SID international symposium digest of technical papers*, pages 731–734. Citeseer, 1996. 8
- [67] Yun Zhang, Linwei Zhu, Gangyi Jiang, Sam Kwong, and C-C Jay Kuo. A survey on perceptually optimized video coding. *ACM Computing Surveys*, 55(12):1–37, 2023. 1
- [68] Hanwei Zhu, Baoliang Chen, Lingyu Zhu, Shiqi Wang, and Weisi Lin. DeepDC: Deep distance correlation as a perceptual image quality evaluator. *CoRR*, abs/2211.04927v2, 2023. 8

Do image and video quality metrics model low-level human vision?

Supplementary Material

This supplementary document provides detailed information on: (S1) the formulas, parameters, and examples of the test stimuli employed in the tests, (S2) a detailed explanation and formulas of the performance measures of each test, and (S3) a summary of the metrics that we evaluated on the different tests, and details of their implementations.

S1. Tests stimuli

Here, we describe the stimuli that were employed for each test and provide their parameters in Tab. S1.

S1.1. Contrast Detection

In contrast detection studies, a contrast pattern, usually presented by a Gabor patch (test image), is compared to a uniform field (reference image). We generated the patterns for different spatial frequencies, temporal frequencies, color modulation, and stimuli radius, depending on each contrast detection test. The reference R and test T stimuli were generated using the following equation:

$$R(x, y) = w_p \cdot L_b \quad \text{and} \quad T(x, y, d, t) = R + G \cdot d_0 \quad (\text{S1})$$

where w_p is the D65 white point in the DKL colorspace, L_b is the background (mean) luminance, d_0 is the cardinal color direction in the DKL space, it is used to define achromatic, red-green (RG), and yellow-violet (YV) stimuli, and G is the Gabor grating defined as follows:

$$G(x, y, t) = c \cdot L_b \cdot \sin\left(2\pi\rho\frac{x}{\text{ppd}}\right) \cdot e^{-\frac{x^2+y^2}{2\text{ppd}^2R^2}} \cdot \cos(2\pi ft) \quad (\text{S2})$$

where ρ is the spatial frequency in cycles per visual degree (cpd), ppd is the effective resolution in the units of pixels per visual degree, R is the stimuli radius in degrees, f is the temporal frequency in Hz, and t is the time in seconds. The x and y are the image coordinates, where $x \in [-\frac{W}{2}, \frac{W}{2}]$ and $y \in [-\frac{H}{2}, \frac{H}{2}]$, where W is the width, and H is the height of the image or frame. For this test, we select a resolution of 1920×1080 and an effective resolution of 60 ppd , to follow with standard viewing conditions. We provide examples of the Gabor stimuli across spatial frequencies in Fig. S1, color in Fig. S2 and Fig. S3, background luminance in Fig. S4, and area in Fig. S5.

S1.2. Contrast Masking

In a contrast masking experiment, a Gabor patch is presented on top of a masker signal (test image), which can be either a sinusoidal grating, for a phase coherent masking, or a broadband noise for a phase incoherent masking,

and compared to the masker (reference image), in order to quantify the contrast threshold for which a contrast can be visible as a function of the masker contrast.

The Sinusoidal grating masker was generated as follows:

$$R(x, y) = L_b \cdot \left(1 + c_m \cdot \cos\left(2\pi\rho_m\frac{x}{\text{ppd}}\right)\right) \quad (\text{S3})$$

where c_m and ρ_m are the masker contrast and the masker spatial frequency, respectively. We have used a cosine function to match the original test. To ensure a phase coherency, we also defined the Gabor patch variation in frequency with a cosine function, and set the x and y image coordinates as $x \in [0, W]$ and $y \in [0, H]$.

The noise masker was generated as follows:

$$R(x, y) = L_b \cdot \left(1 + c_m \cdot \frac{N_{bp}}{\sigma_{N_{bp}}}\right) \quad (\text{S4})$$

where c_m is the masker contrast and N_{bp} is the broadband noise pattern expressed as:

$$N_{bp}(x, y) = \Re(\mathcal{F}^{-1}(\mathcal{F}(N)(\rho_m \geq 12))) \quad (\text{S5})$$

where $\mathcal{F}(\cdot)$ is the Fourier transform, ρ_m is the masker spatial frequency between 0 and 12 cpd, N is a 2D Gaussian noise for the image coordinates $x \in [0, W]$ and $y \in [0, H]$. We ensured that the noise was fixed over all metrics and stimuli by fixing the seed parameter.

We provide examples of the phase coherent contrast masking test stimuli in Fig. S6 and the phase incoherent test stimuli in Fig. S7.

S1.3. Flicker Detection

The flicker detection test follows the same methodology as a contrast detection test, where a flickering disk is compared to a uniform field. The flickering disk is expressed as follows:

$$R(x, y, t) = L_b(1 + c \cdot D \cdot \sin(2\pi ft)) \quad (\text{S6})$$

where c is the disk contrast, L_b is the background luminance, f is the temporal frequency, and D is the disk. The disk equation is expressed as follows:

$$\frac{x^2}{\text{ppd}^2} + \frac{y^2}{\text{ppd}^2} \leq R^2 \quad (\text{S7})$$

where R is the disk radius.

Contrary to Eq. (S2), we employ a sine instead of a cosine function to model the temporal variation, as in this test, we are not interested in detecting the disk; rather, we are interested in detecting the flicker.

Example videos of the flicker test stimuli can be found in the supplementary HTML report.

Table S1. A summary of the tests’ parameters. Tests which use a sinusoidal gratings do not have a radius. The disk in the flicker test do not have a spatial frequency. The resolution of the stimuli can be estimated from the effective resolution and the visual field size. The effective resolution of the contrast detection across spatial frequencies have been set to 66 ppd, as we are testing frequencies up tp 32 cpd. Furthermore, we set the effective resolution of the contrast matching across spatial frequencies to 50 ppd as we are testing frequencies up to 25 cpd.

Test	Contrast	Spatial Frequency [cpd]	Mean Luminance [cd/m ²]	Stimuli Radius [°]	Temporal Frequency [Hz]	Effective Resolution [ppd]	Field Size [H×V]
Contrast Detection Spatial Freq. - Ach. Gabor	0.001 - 1	0.5 - 32	21.4	2	0	66	29° × 16.4°
Contrast Detection Spatial Freq. - RG Gabor	0.001 - 0.12	0.5 - 32	21.4	2	0	66	29° × 16.4°
Contrast Detection Spatial Freq. - YV Gabor	0.01 - 0.8	0.5 - 32	21.4	2	0	66	29° × 16.4°
Contrast Detection Spatial Freq. - Ach Transient Gabor	0.001 - 1	0.5 - 32	21.4	2	8	66	3.9° × 3.9°
Contrast Detection - Luminance	0.001 - 1	2	0.1 - 90	2	0	60	32° × 18°
Contrast Detection - Area	0.001 - 1	2	21.4	0.25 - 8	0	60	32° × 18°
Contrast Masking - Phase Coherent	0.005 - 0.5	2 (test) / 2 (mask)	32	0.5	0	60	7° × 5°
Contrast Masking - Phase Incoherent	0.005 - 0.5	1.2 (test) / 0-12 (mask)	37	0.8	0	60	5° × 5°
Flicker Detection	0.001 - 1	-	21.4	2	0 - 60	60	4.3° × 4.3°
Contrast Matching - Spatial Freq.	0.005 - 0.629 (ref) / 0.001 - 1 (test)	5 (ref) / 0.25 - 25 (test)	10	-	0	50	5.1° × 5.1°
Contrast Matching - Color Directions	0.01 - 0.2 (ach. ref)	1	21.4	-	0	60	4.3° × 4.3°

S1.4. Contrast Matching

In a contrast matching experiment, two contrast patterns presented as sinusoidal gratings are presented to the observer to be matched. The sinusoidal grating is generated as follows:

$$T(x, y) = L_b \cdot \left(1 + c \cdot \sin \left(2\pi\rho \frac{x}{\text{ppd}} \right) \right) \quad (\text{S8})$$

where L_b is the background luminance, c is the contrast, ρ is the spatial frequency, and ppd is the effective resolutions.

However, in the contrast matching across cardinal color directions test, a horizontal sinusoidal grating was presented instead, as follows:

$$T(x, y, d) = L_b \cdot \left(w_p + c \cdot \sin \left(2\pi\rho \frac{y}{\text{ppd}} \right) \cdot d_0 \right) \quad (\text{S9})$$

Here, we are generating the grating in the DKL color space in order to model the color directions, where w_p is the whitepoint and d_0 is the color direction.

We provide examples of the stimuli employed for the contrast matching across spatial frequencies test in Fig. S8 and across cardinal color directions test in Fig. S9.

S2. Performance measures

We use contour plot and matching contrast line visualizations as the primary tools for investigating metric performance. However, to show a high-level overview across multiple metrics, we also calculate summative performance measures.

Alignment score for detection and masking For both detection and masking tests, we employ the alignment score introduced in [6], which we describe here for completeness.

We are interested in how well the metrics’ predictions follow the contrast threshold. A metric that aligns with the psychophysical data should predict the same quality score at the contrast threshold. However, this can be a weak measure, as metrics can predict the same maximum score if it does not detect the contrast (or flicker). Hence, we evaluate the metrics predictions at the neighbors of a given contrast threshold. We sample 10 multipliers m_i ranging from 0.5 to 2 and obtain neighboring contrast levels by multiplying the detection threshold with the multipliers m_i . If a metric performs well, it will predict the same quality score for the same multiplier; however, it will also predict different scores at different multipliers. The alignment score is defined as the Spearman rank-order correlation between the multiplier value and the metrics predictions.

RMSE for contrast matching In the matching tests, we are interested in observing how well the predicted contrasts (after matching with the reference) align with the ground truth. Hence, for the contrast matching across spatial frequencies test, we employ an RMSE in log space between the predicted test contrasts and the ground-truth test contrasts.

In the contrast matching across cardinal color directions test, we want to measure how well the predictions align across the color directions. For this purpose, we employ an RMSE between the metrics’ predictions of the stimuli across the achromatic, RG, and YV channels. However, since metrics’ predictions follow different scales, we normalize the differences by scaling them using the maximum and minimum of the overall predictions, before calculating

the RMSE, as shown in the following equation:

$$\text{RMSE} = \sqrt{\sum_c \frac{1}{N} \frac{\sum_{d=1}^2 (Q_{c,d} - Q_{c,d+1})^2}{(\max_{c,d} Q_{c,d} - \min_{c,d} Q_{c,d})^2}} \quad (\text{S10})$$

with

$$Q_{c,d} = Q(S(c, d), U) \quad (\text{S11})$$

where Q is the quality prediction of a specific metric, S is the stimulus, defined by a contrast c , and a color direction d for Achromatic, RG, and YV, U is a uniform field, and N is the total number of tested contrast values. In our framework, we defined $N = 10$.

S3. Metrics

We selected 33 full-reference image and video quality metrics to evaluate their performance on the proposed tests. Details on the metrics are provided in Tab. S2. Most metrics were run on PyTorch using the PIQ [14] and PyIQA [7] toolboxes to ensure that we provide them with floating point numbers. For other metrics, which required YUV files, we quantized them to 16 bits to minimize the loss of information.

References

- [1] Saeedeh Abasi, Mohammad Amani Tehran, and Mark D Fairchild. Distance metrics for very large color differences. *Color Research & Application*, 45(2):208–223, 2020. 4
- [2] Pontus Andersson, Jim Nilsson, Tomas Akenine-Möller, Magnus Oskarsson, Kalle Åström, and Mark D Fairchild. FLIP: A difference evaluator for alternating images. *Proc. ACM Comput. Graph. Interact. Tech.*, 3(2):15–1, 2020. 4
- [3] Amnon Balanov, Arik Schwartz, Yair Moshe, and Nimrod Peleg. Image quality assessment based on dct subband similarity. In *ICIP*, pages 2105–2109. IEEE, 2015. 4
- [4] Christos G Bampis, Praful Gupta, Rajiv Soundararajan, and Alan C Bovik. SpEED-QA: Spatial efficient entropic differencing for image and video quality. *IEEE signal processing letters*, 24(9):1333–1337, 2017. 4
- [5] Sebastian Bosse, Dominique Maniry, Klaus-Robert Müller, Thomas Wiegand, and Wojciech Samek. Deep neural networks for no-reference and full-reference image quality assessment. *IEEE TIP*, 27(1):206–219, 2017. 4
- [6] Yancheng Cai, Fei Yin, Dounia Hammou, and Rafal Mantiuk. Do computer vision foundation models learn the low-level characteristics of the human visual system? (arXiv:2502.20256), 2025. arXiv:2502.20256 [cs]. 2
- [7] Chaofeng Chen and Jiadi Mo. IQA-PyTorch: Pytorch toolbox for image quality assessment. [Online]. Available: <https://github.com/chaofengc/IQA-PyTorch>, 2022. 3
- [8] Chaofeng Chen, Jiadi Mo, Jingwen Hou, Haoning Wu, Liang Liao, Wenxiu Sun, Qiong Yan, and Weisi Lin. TOPIQ: A top-down approach from semantics to distortions for image quality assessment. *IEEE TIP*, 2024. 4
- [9] CIE. CIE 015: 2018 Colorimetry, 2018. 4
- [10] Keyan Ding, Kede Ma, Shiqi Wang, and Eero P Simoncelli. Image quality assessment: Unifying structure and texture similarity. *IEEE TPAMI*, 44(5):2567–2581, 2020. 4
- [11] Abhijay Ghildyal and Feng Liu. Shift-tolerant perceptual similarity metric. In *ECCV*, pages 91–107. Springer, 2022. 4
- [12] Jiaqi He, Zhihua Wang, Leon Wang, Tsein-I Liu, Yuming Fang, Qilin Sun, and Kede Ma. Multiscale sliced Wasserstein distances as perceptual color difference measures. In *ECCV*, pages 1–18, 2024. 4
- [13] ITU-R. BT.2124-0: Objective metric for the assessment of the potential visibility of colour differences in television, 2019. 4
- [14] Sergey Kastyulin, Dzhamil Zakirov, and Denis Prokopenko. PyTorch Image Quality: Metrics and measure for image quality assessment, 2019. Open-source software available at <https://github.com/photosynthesis-team/piq>. 3
- [15] Shanshan Lao, Yuan Gong, Shuwei Shi, Sidi Yang, Tianhe Wu, Jiahao Wang, Weihao Xia, and Yujiu Yang. Attention help CNNs see better: Attention-based hybrid image quality assessment network. In *CVPR*, pages 1140–1149, 2022. 4
- [16] Valero Laparra, Johannes Ballé, Alexander Bernardino, and Eero P Simoncelli. Perceptual image quality assessment using a normalized laplacian pyramid. *Electronic Imaging*, 28: 1–6, 2016. 4
- [17] Eric C Larson and Damon M Chandler. Most apparent distortion: full-reference image quality assessment and the role of strategy. *Journal of electronic imaging*, 19(1):011006–011006, 2010. 4
- [18] Zhi Li, Christos Bampis, Julie Novak, Anne Aaron, Kyle Swanson, Anush Moorthy, and JD Cock. VMAF: The journey continues. *Netflix Technology Blog*, 25(1), 2018. 4
- [19] Rafał K Mantiuk, Gyorgy Denes, Alexandre Chapiro, Anton Kaplanyan, Gizem Rufo, Romain Bachy, Trisha Lian, and Anjul Patney. FovVideoVDP: A visible difference predictor for wide field-of-view video. *ACM TOG*, 40(4):1–19, 2021. 4
- [20] Rafal K Mantiuk, Dounia Hammou, and Param Hanji. HDR-VDP-3: A multi-metric for predicting image differences, quality and contrast distortions in high dynamic range and regular content. *arXiv preprint arXiv:2304.13625*, 2023. 4
- [21] Rafal K. Mantiuk, Param Hanji, Maliha Ashraf, Yuta Asano, and Alexandre Chapiro. ColorVideoVDP: A visual difference predictor for image, video and display distortions. *ACM TOG*, 43(4), 2024. 4
- [22] Hossein Ziaei Nafchi, Atena Shahkolaei, Rachid Hedjam, and Mohamed Cheriet. Mean deviation similarity index: Efficient and reliable full-reference image quality evaluator. *IEEE Access*, 4:5579–5590, 2016. 4
- [23] Rafael Reisenhofer, Sebastian Bosse, Gitta Kutyniok, and Thomas Wiegand. A Haar wavelet-based perceptual similarity index for image quality assessment. *Signal Processing: Image Communication*, 61:33–43, 2018. 4
- [24] Hamid R Sheikh and Alan C Bovik. Image information and visual quality. *IEEE TIP*, 15(2):430–444, 2006. 4

Table S2. A summary of the metrics employed in the evaluation. The “color” column states if the metric accounts for colors. The “temporal” column states if the metric considers temporal information, and the “CSF-based” column indicates whether the metric is designed using the CSF.

Metric	Color	Temporal	CSF-Based	Details
PSNR-Y	No	No	No	Mathematical measure of the pixel-wise difference.
SSIM [27]	No	No	No	Measure of difference in luminance, contrast, and structural information.
MS-SSIM [26]	No	No	No	Multi-scale variant of SSIM.
GMSD [28]	No	No	No	Gradient magnitude similarity measure.
MS-GMSD [29]	No	No	No	Multi-scale variant of GMSD.
VIFp [24]	No	No	No	Measure of the loss of information.
DSS [3]	No	No	No	DCT subbands’ similarity measure.
NLPD [16]	No	No	No	Distance measure of the Laplacian pyramid’s normalized contrast.
FSIMc [30]	Yes	No	No	A phase congruency and gradients’ magnitude similarity measure.
VSI [31]	Yes	No	No	Visual saliency-based weighting of features’ similarity.
MDSI [22]	Yes	No	No	A gradient and chromaticity similarity measure.
HaarPSI [23]	Yes	No	No	A Haar wavelet coefficients’ similarity measure.
sCIELab [33]	Yes	No	Yes	A CSF-based difference measure in the CIELab color space.
FLIP [2]	Yes	No	Yes	Fusion of color and feature differences in a perceptual uniform space.
CIEDE2000 [9]	Yes	No	No	A perceptual color measure in the CIELab color space.
HyAB [1]	Yes	No	No	A taxicab distance between the lightness and chroma in the CIELab color space.
Dolby ICtCp [13]	Yes	No	No	A color measure in the ICtCp color space.
MS-SWD [12]	Yes	No	No	A multiscale sliced wasserstein distance color measure.
WaDIQaM [5]	Yes	No	No	A deep neural network trained end-to-end for quality assessment.
LPIPS [32]	Yes	No	No	A difference measure of the activations of a deep neural network (Alex and VGG Nets).
ST-LPIPS [11]	Yes	No	No	An LPIPS-based metric tolerant to imperceptible shifts
DISTS [10]	Yes	No	No	A DNN-based model tolerant to texture resampling.
AHIQ [15]	Yes	No	No	A hybrid model of CNN and ViT for quality assessment.
TOPIQ [8]	Yes	No	No	A CNN-based model for high-level semantic information extraction for quality assessment.
DeepDC [34]	Yes	No	No	A distance correlation between the deep features.
VMAF [18]	No	Yes	Yes	A fusion of VIF, DLM, and temporal information metrics.
SpeedQA [4]	No	Yes	No	A multi-scale measure of spatial and temporal entropic information differences.
FUNQUE [25]	No	Yes	Yes	An efficient fusion of improved VIF, DLM, ESSIM, and temporal information metrics.
MAD [17]	No	No	Yes	A combination of near and supra threshold detection in quality metrics.
HDR-VDP-3 [20]	No	No	Yes	A visual different predictor based on low-level human vision for image distortions.
FovVideoVDP [19]	No	Yes	Yes	A visual different predictor based on spatial, temporal, and peripheral low-level human vision.
ColorVideoVDP [21]	Yes	Yes	Yes	A visual different predictor based on spatial, temporal, and chromatic low-level human vision.

[25] Abhinav K Venkataramanan, Cosmin Stejerean, and Alan C Bovik. FUNQUE: Fusion of unified quality evaluators. In *ICIP*, pages 2147–2151. IEEE, 2022. 4

[26] Zhou Wang, Eero P Simoncelli, and Alan C Bovik. Multiscale structural similarity for image quality assessment. In *Asilomar Conference on Signals, Systems & Computers*, pages 1398–1402. IEEE, 2003. 4

[27] Zhou Wang, Alan C Bovik, Hamid R Sheikh, and Eero P Simoncelli. Image quality assessment: from error visibility to structural similarity. *IEEE TIP*, 13(4):600–612, 2004. 4

[28] Wufeng Xue, Lei Zhang, Xuanqin Mou, and Alan C Bovik. Gradient magnitude similarity deviation: A highly efficient perceptual image quality index. *IEEE TIP*, 23(2):684–695, 2013. 4

[29] Bo Zhang, Pedro V Sander, and Amine Bermak. Gradient magnitude similarity deviation on multiple scales for color image quality assessment. In *ICASSP*, pages 1253–1257. IEEE, 2017. 4

[30] Lin Zhang, Lei Zhang, Xuanqin Mou, and David Zhang. FSIM: A feature similarity index for image quality assessment. *IEEE TIP*, 20(8):2378–2386, 2011. 4

[31] Lin Zhang, Ying Shen, and Hongyu Li. VSI: A visual

saliency-induced index for perceptual image quality assessment. *IEEE TIP*, 23(10):4270–4281, 2014. 4

[32] Richard Zhang, Phillip Isola, Alexei A Efros, Eli Shechtman, and Oliver Wang. The unreasonable effectiveness of deep features as a perceptual metric. In *CVPR*, 2018. 4

[33] Xuemei Zhang, Brian A Wandell, et al. A spatial extension of CIELAB for digital color image reproduction. In *SID international symposium digest of technical papers*, pages 731–734. Citeseer, 1996. 4

[34] Hanwei Zhu, Baoliang Chen, Lingyu Zhu, Shiqi Wang, and Weisi Lin. DeepDC: Deep distance correlation as a perceptual image quality evaluator. *CoRR*, abs/2211.04927v2, 2023. 4

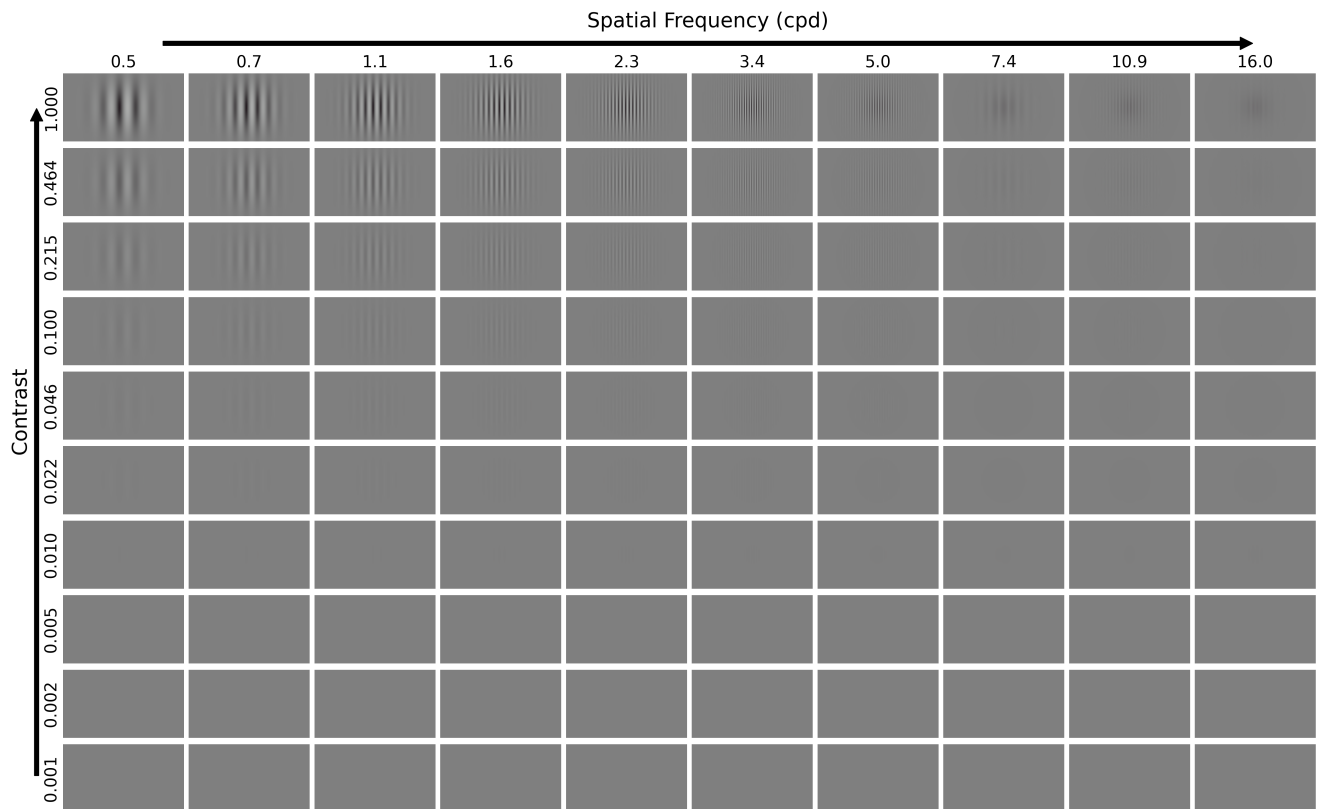


Figure S1. A representation of the test images used in the contrast detection across spatial frequencies test. We showcase the achromatic Gabor patches (test images) across spatial frequency (x-axis) and contrast (y-axis). In the test, we employed spatial frequencies up to 32 cpd (cycles per visual degree); however, we show them up to 16 cpd in the figure, as higher-frequency patterns may introduce aliasing artifacts on screen or print (these aliasing artifacts were not present in the test).

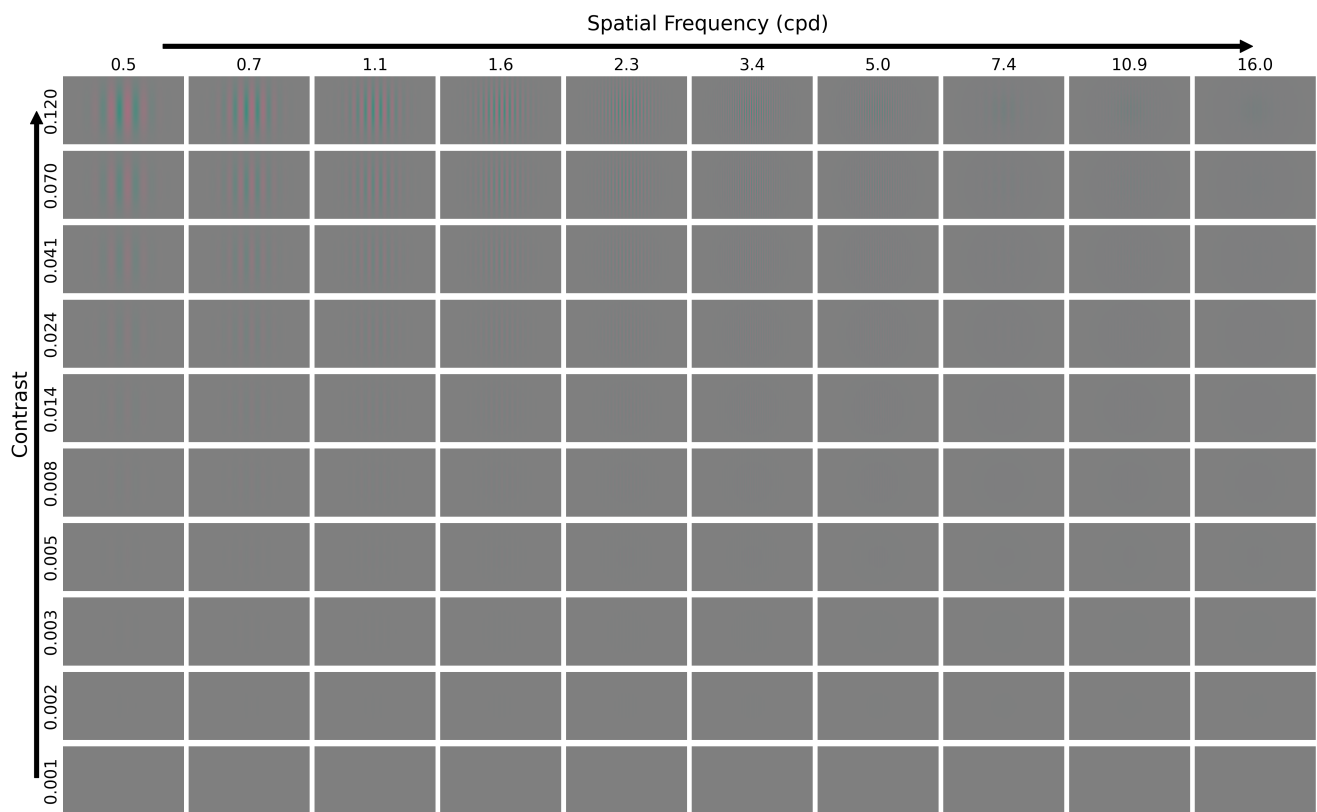


Figure S2. A representation of the test images used in the contrast detection across spatial frequencies test. We showcase the red-green (RG) Gabor patches (test images) across spatial frequency (x-axis) and contrast (y-axis).

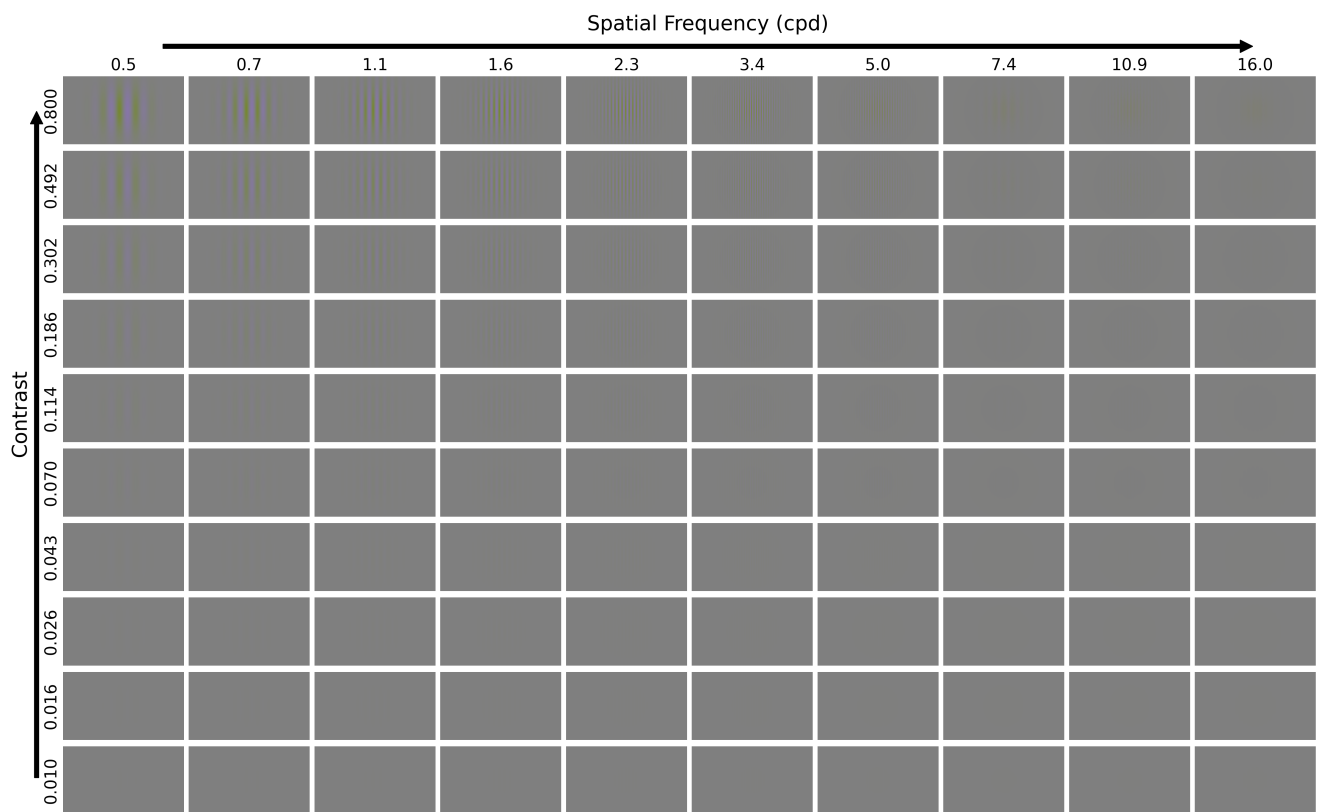


Figure S3. A representation of the test images used in the contrast detection across spatial frequencies test. We showcase the yellow-violet (YV) Gabor patches (test images) across spatial frequency (x-axis) and contrast (y-axis).

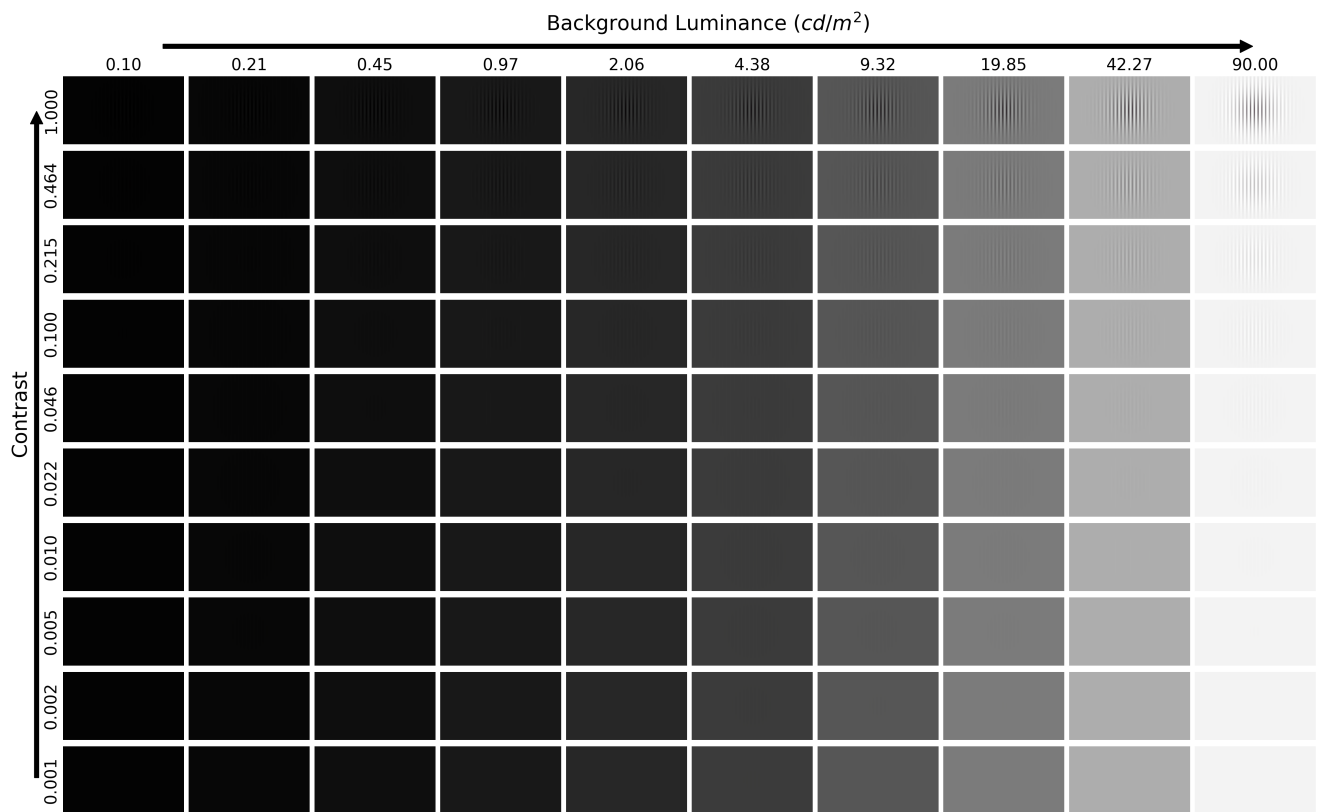


Figure S4. A representation of the test images used in the contrast detection across background luminance test. We showcase the achromatic Gabor patches (test images) across background luminance (x-axis) and contrast (y-axis).

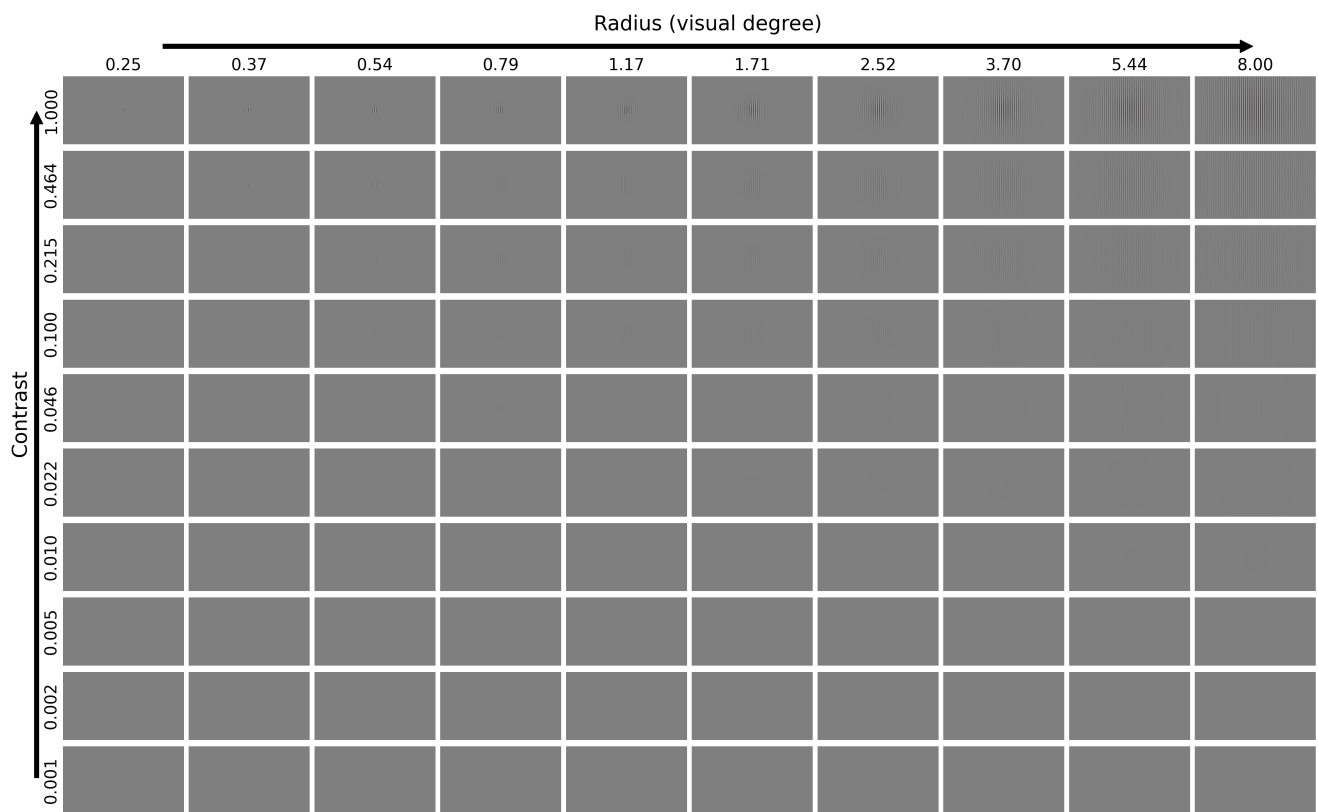


Figure S5. A representation of the test images used in the contrast detection across area test. We showcase the achromatic Gabor patches (test images) across Gabor Radius (x-axis) and contrast (y-axis).

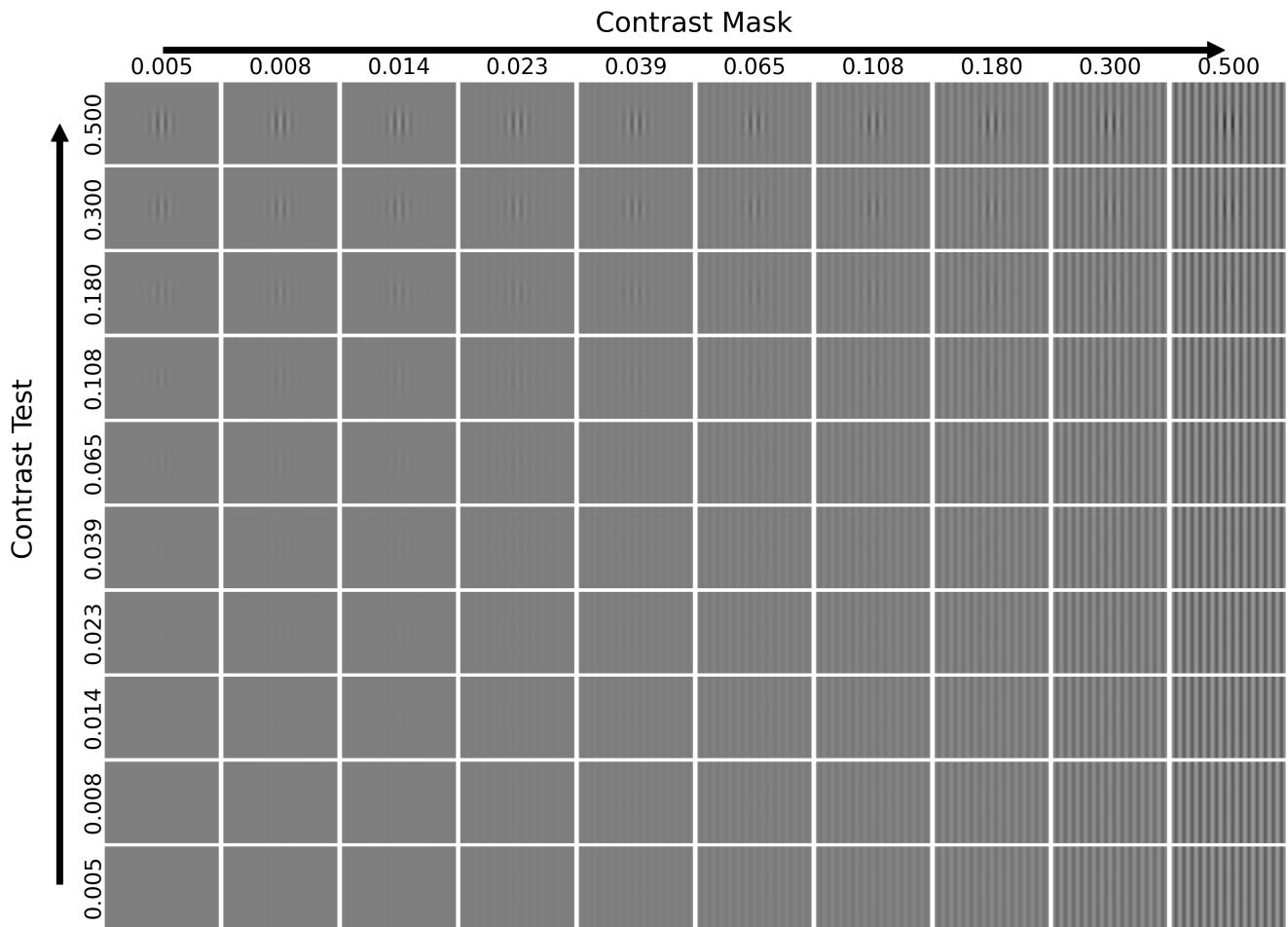


Figure S6. A representation of the test images used in the phase coherent contrast masking. We showcase the achromatic Gabor patches on top of sinusoidal gratings (test images) across mask contrast (x-axis) and test contrast (y-axis).

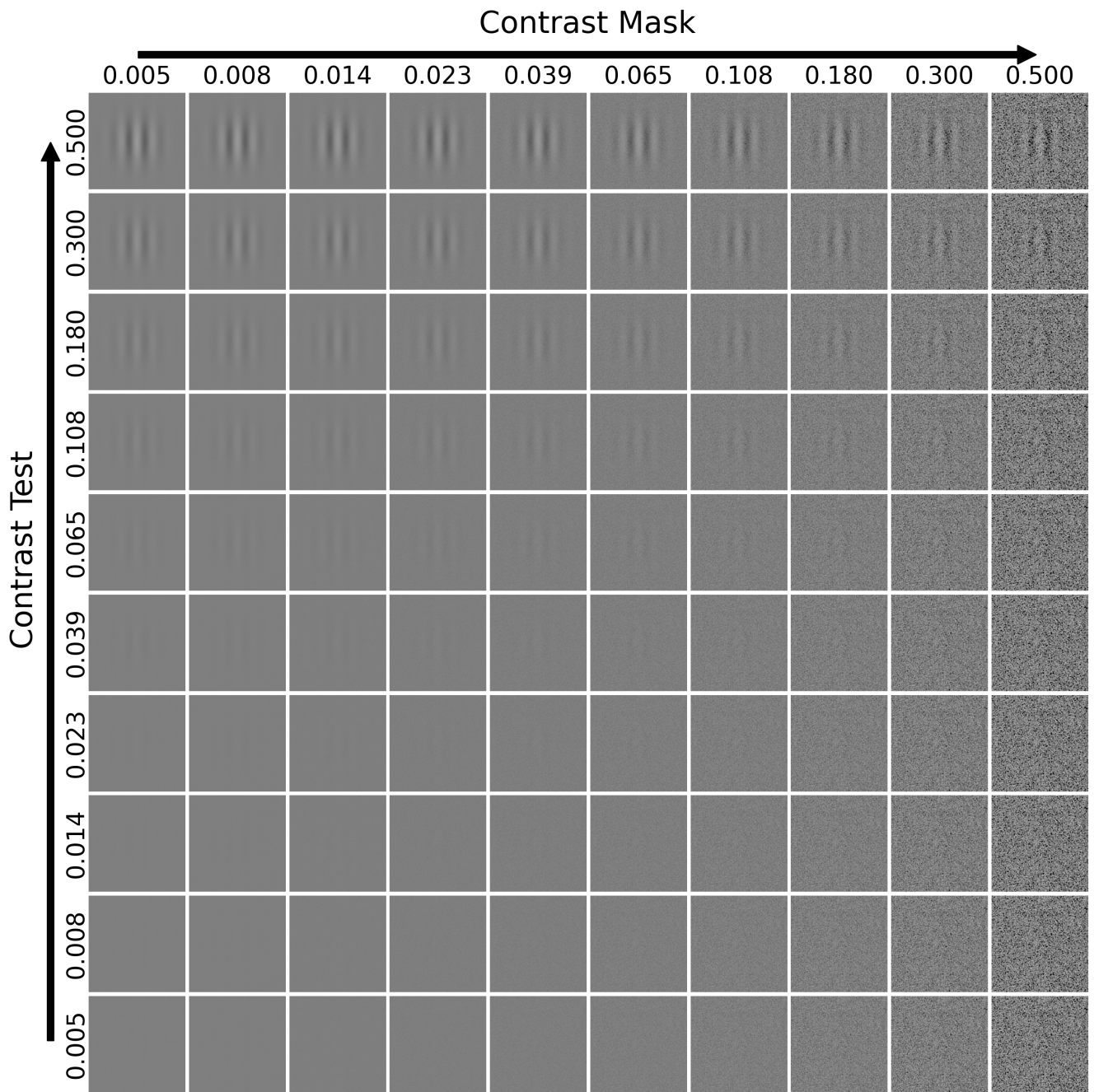


Figure S7. A representation of the test images used in the phase incoherent contrast masking. We showcase the achromatic Gabor patches on top of broadband noise (test images) across masker contrast (x-axis) and test contrast (y-axis).

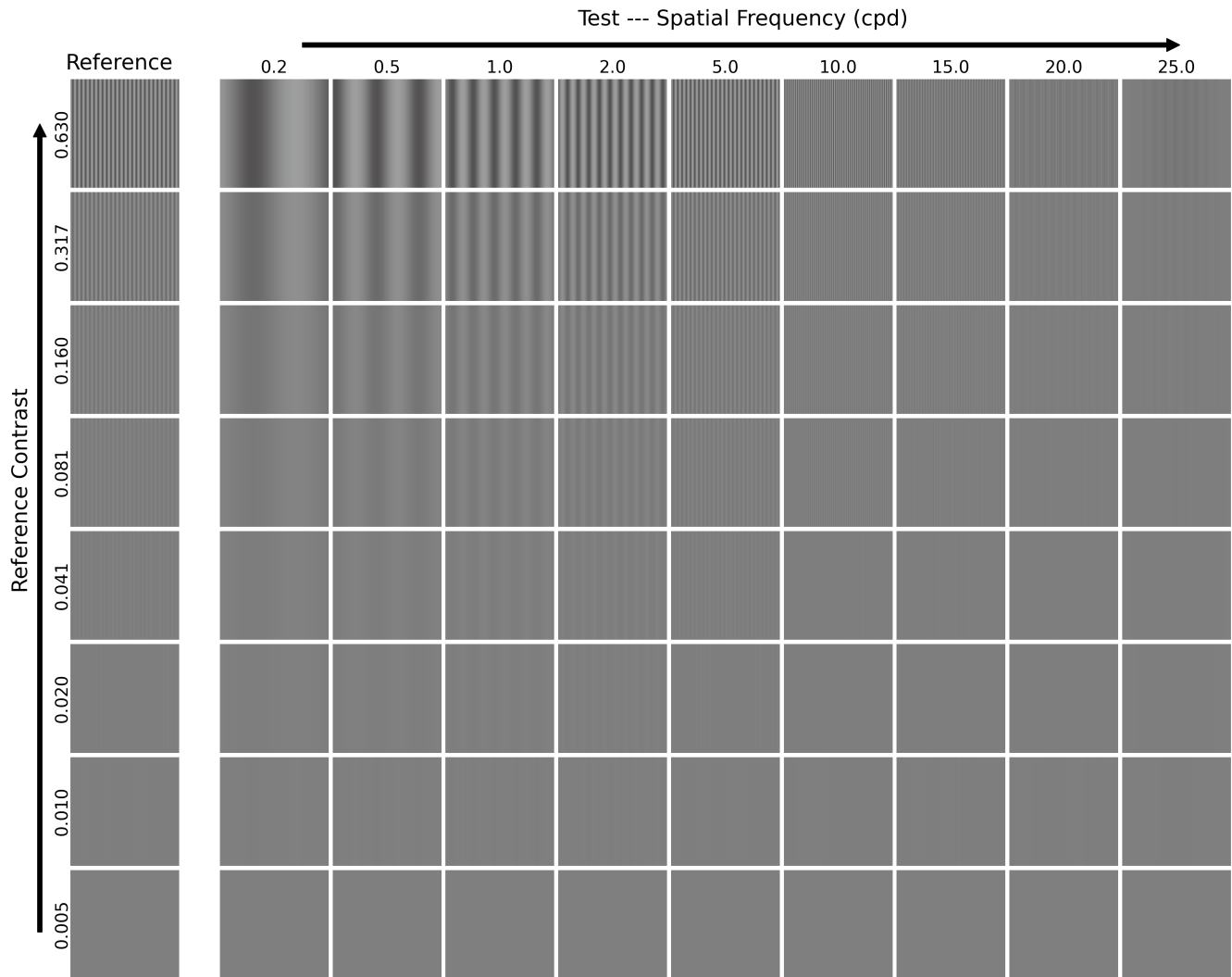


Figure S8. A representation of the test and reference images used in the contrast matching across spatial frequencies test. We showcase the reference images on the left, generated for multiple reference contrast and a spatial frequency of 5 cpd. The test images are presented in the grid across spatial frequency (x-axis) and reference contrast (y-axis).

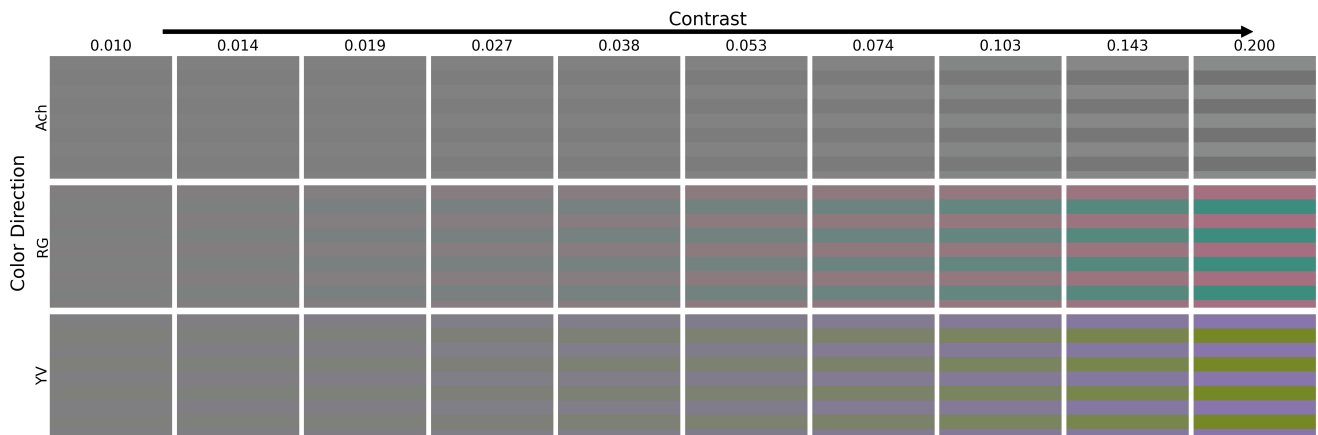


Figure S9. A representation of the test images used in the contrast matching across cardinal color directions. We showcase the sinusoidal grating across contrast (x-axis) and color directions (y-axis). The contrast of the RG and YV stimuli were selected to match that of the achromatic stimulus.